Crystallization Behavior of Poly(ethylene oxide) and Its Blends Using Time-Resolved Wide- and Small-Angle X-ray Scattering

Melissa S. Lisowski,† Qiang Liu,‡ Jaedong Cho, and James Runt*

Department of Materials Science and Engineering, The Pennsylvania State University, University Park, Pennsylvania 16802

Fengji Yeh and Benjamin S. Hsiao

Department of Chemistry, State University of New York at Stony Brook, Stony Brook, New York 11794

Received February 3, 2000; Revised Manuscript Received April 26, 2000

ABSTRACT: Time-resolved synchrotron wide- and small-angle X-ray scattering experiments were used to investigate the crystallization behavior and microstructure development of poly(ethylene oxide) and several melt-miscible PEO blends. Model blends were prepared with both weakly interacting poly(methyl methacrylate) and two strongly interacting random copolymers. Average SAXS long periods and lamellar thicknesses decreased at early crystallization times: by 2−3 nm for PEO and blends containing the low T_g diluent and by ∼5−9 nm for blends containing higher T_g diluents. The latter appears to arise in part from additional restrictions placed on the growing lamellae by the stiff, high T_g amorphous polymeric diluents. The increase in final long period over that of neat PEO was ∼2−4 nm for the weakly interacting blends, as opposed to as large as 10 nm for the strongly interacting mixtures. In the former case, the changes are associated with interlamellar diluent placement, while in the latter they result primarily from an increase in lamellar thickness due to reduction in degrees of supercooling. In line with previous observations, there was a significant decrease in crystallization rates for blends containing strongly interacting diluents. Two Avrami expressions were generally required to fit the WAXD crystallinity−time data for PEO and as many as three for the blends. For neat PEO, the behavior is reminiscent of crystallization in mixtures of high and low molecular weight PEO fractions.

Introduction

We have recently undertaken a series of experimental studies directed at determining the final microstructure and spherulitic crystallization of a series of "model" melt-miscible blends.[1−3] Poly(ethylene oxide) [PEO] was chosen as the semicrystalline component for these studies since it exhibits miscibility in the melt with a relatively broad range of polymers. Several miscible amorphous polymeric diluents were used in order to focus on the role of diluent mobility and on the role of strong intermolecular interactions.

Most recently, spherulite growth rates for the model blend systems, acquired over a range of crystallization temperatures (T_c) and compositions, were analyzed.[3] For blends crystallized at most T_c's, typical linear spherulite radius vs time behavior was observed, indicative of a constant composition at the crystal growth front during the crystallization process. The implication is that the crystallization rate is faster than the rate of diffusion of the amorphous polymer away from the growth front, thereby trapping the diluent polymer in the crystalline microstructure.[4,5] However, nonlinear growth was observed for some blends, particularly those containing strongly interacting polymers and crystallized at relatively low degrees of supercooling (ΔT). This behavior indicates an increasing concentration of diluent polymer in the uncrystallized phase as crystallization proceeds and hence a slower spherulite growth rate. At relatively short crystallization times, the development of the spherulite radius (R) was found to be directly proportional to time (and hence the growth rate, G, is constant), whereas there is a crossover to diffusion-controlled growth at longer times to $R \propto t^{1/2}$ ($G \propto t^{-1/2}$).

At a given T_c, growth rates for melt-miscible PEO blends with strongly interacting amorphous polymers were found to be considerably lower than both neat PEO and blends with weakly interacting polymers having comparable glass transition temperatures (T_g). An important part of this decrease is related to the depression of the equilibrium melting point (T_m^0) of the PEO in these mixtures. Growth rates for PEO and blends with low and high T_g diluent polymers could be superposed to give reasonable "master curve" behavior when normalized by ΔT ($= T_m^0 - T_c$) and a simple term proportional to the transport of the crystallizable species to the growth front.[3]

Although these optical microscopy experiments provided valuable information on crystallization of PEO in the presence of various diluent polymers at the spherulite level, they do not provide any insight into the course of crystallization at the lamellar level, nor do they reveal how the degree of crystallinity develops during crystallization. Both of these factors are important to our fundamental understanding of blend crystallization. Consequently, in the present paper we focus on bulk crystallization and microstructure formation (via time-resolved small- and wide-angle X-ray scattering experiments) of our model PEO blends. There have been a modest number of real-time scattering experiments conducted previously on crystalline polymer blends (e.g., refs 6−9). However, aside from our early report,[2] there have been few systematic studies in which the component polymers exhibit strong intermolecular interactions. Two such blend systems have been included in

† Current address: Montell Polyolefins, Elkton, MD 21921.
‡ Current address: Agriculture and Agri-Food Canada, Guelph, Ontario, Canada N1G 2W1.

10.1021/ma000207c CCC: $19.00
Published on Web 05/24/2000

Table 1. Materials and Crystallization Temperatures

material	T_c (°C)	material	T_c (°C)
PEO	45, 48, 50, 52	85/15 EMAA	48
80/20 PEO/PMMA	45, 48	90/10 PEO/SHS	45, 48
90/10 PEO/EMAA	45, 48	80/20 SHS	45, 48

our studies, as well as one in which the component polymers exhibit relatively weak intermolecular interactions.

Experimental Section

Materials. The polymers used in this study were identical to those used in our previous work.[1−3] The PEO had $M_w = 1.81 \times 10^5$ (relative to PEO molecular weight standards) and a polydispersity index of 3.9. The weakly interacting amorphous polymer used in these experiments, poly(methyl methacrylate) [PMMA], was purchased from Aldrich and had a measured $T_g = 113$ °C. The amorphous polymers exhibiting strong intermolecular interactions with PEO are (1) a random copolymer of ethylene and methacrylic acid (EMAA, 55 wt % acid units) and (2) a random copolymer of styrene and hydroxystyrene (SHS, 50 wt % hydroxystyrene). These copolymers had T_g's of 36 and 150 °C and were supplied respectively by duPont[10] and Hoechst Celanese. Other detailed information for the amorphous polymers is summarized in ref 1.

Selected blend compositions were prepared by casting from 2 wt % solutions: PEO/PMMA blends from $CHCl_3$ and PEO/SHS and PEO/EMAA blends from a 50/50 solution of THF and CH_2Cl_2. The cast films were dried at room temperature for 48 h and then in a vacuum oven for 6 h at 90 °C. The films were then placed in a Carver hydraulic press for 2 min at 100 °C and 20 000 lb and then rapidly cooled in air. PEO films were prepared by pressing powdery PEO under the same conditions as the blends. Samples for simultaneous wide-angle X-ray diffraction (WAXD) and small-angle X-ray scattering (SAXS) experiments were prepared by cutting films into small circular pieces, depositing them into a copper cell, heating to 90 °C, and applying light pressure by hand with a metal insert to consolidate them. Samples were approximately 7 mm in diameter and 2 mm in thickness.

Time-Resolved WAXD/SAXS. The time-resolved simultaneous WAXD/SAXS experiments were conducted at the National Synchrotron Light Source, Brookhaven National Laboratory on the Advanced Polymers Beamline, X27C. The X-ray wavelength was 0.1307 nm, and pinhole collimation was utilized. Two linear gas-filled delay-line position-sensitive detectors connected in series were used to collect the SAXS and WAXD data simultaneously. For SAXS, the sample to detector distance was 1.19 m, covering an angular range up to $q \sim 1.5$ nm^{-1} [q is the scattering vector and $q = 4\pi/\lambda \sin\theta$ where λ is the wavelength and 2θ the scattering angle]. The WAXD 2θ range was ~16°−31° (relative to $\lambda = 0.154$ nm). The scattering from a duck tendon and a Lupolen standard were used to calibrate the SAXS and WAXD detectors, respectively. Details of the beamline setup are provided in ref 11.

Real-time WAXD/SAXS experiments on the crystallization of PEO and selected blends were conducted using a specially designed sample holder to allow for a rapid jump between the melt temperature and selected T_c's.[11] Since the thermal chambers were well insulated and the temperature jump was relatively small in our case (from 100 °C to the crystallization temperature, ~55 °C), it was estimated that the sample reached T_c in ~1 min. This time scale was shorter than the induction time for the appearance of wide-angle diffraction pattern at the lowest T_c used here. Time-resolved WAXD/SAXS experiments were conducted during crystallization of the samples listed in Table 1.

Degrees of crystallinity were determined from WAXD data using a curve-fitting program where the diffraction profile was separated into three crystalline PEO reflections and an amorphous halo.[12] The apparent degree of crystallinity was defined as the ratio of the area under the resolved crystalline peaks to the total unresolved area.

The SAXS data were first smoothed using a moving window averaging procedure,[13] and then background scattering due to thermal density fluctuations was subtracted using the procedure described in ref 13. The one-dimensional correlation function was calculated from all scattering curves:[14]

$$\gamma(r) = \int_0^\infty q^2 I(q) \cos(qr)\, dq \tag{1}$$

where r is the correlation distance. The relative invariant (Q') was obtained as the ordinate of the linear fit to the self-correlation portion of the correlation function. For an ideal two-phase system with well-defined interfaces, the invariant per unit scattering volume is related to the difference between the electron densities of the crystalline and amorphous regions by

$$Q' = K v_s x_c (1 - x_c) \Delta\eta^2 \tag{2}$$

where K is a constant depending on the experimental conditions, x_c is the linear crystallinity (given by the ratio of the lamellar thickness, l_c, to the average long period, L), v_s is the volume fraction of lamellar stacks (given by the ratio of the bulk crystallinity to the linear crystallinity), and $\Delta\eta$ is the linear electron density difference defined as $\Delta\eta = \eta_c - \eta_a$, where η_c and η_a are the electron densities of the crystal and amorphous layers, respectively.

If B is the value of the abscissa where the ordinate first equals zero in $\gamma(r)$, and the long period is obtained from the first maximum of $\gamma(r)$, then $x_c(1 - x_c) = B/L$. Although one cannot apriori distinguish x_c from x_a ($= 1 - x_c$), it was shown in our earlier work that x_c for neat PEO was greater than 0.7.[1] Since lamellar thicknesses for the strongly interacting blends are greater than those of PEO at the same T_c and these diluents reside primarily outside of lamellar stacks,[1] the larger values calculated for x_c for these blends can also be safely assumed to be the correct ones. The average lamellar thickness can then be calculated from $l_c = x_c L$. Likewise, the average amorphous layer thickness within lamellar stacks can be obtained from $l_a = (1 - x_c)L$.

Results and Discussion

For clarity, the WAXD/SAXS results for neat PEO are discussed first. This is followed by a discussion of the behavior of the blends, first at $T_c = 45$ °C and then $T_c = 48$ °C. A summary is provided at the end of the paper in order to highlight the important points.

Poly(ethylene oxide). Development of the lamellar microstructure and bulk crystallinity of neat PEO was followed at four crystallization temperatures: 45, 48, 50, and 52 °C. Figure 1 shows the WAXD and SAXS profiles at selected times for crystallization at 45 °C. The general behavior of PEO (and the blends) crystallized at different temperatures was similar to that shown in Figure 1. No systematic changes in the positions of the WAXD crystalline reflections or the widths at half peak height were noted during the crystallization of either neat PEO or PEO in the blends. A second-order reflection is apparent in the SAXS profiles of the neat PEO (see Figure 1b for example), indicative of relatively well ordered lamellar stacks.

The time-dependent WAXD crystallinities for the four PEO crystallization experiments are shown in Figure 2a. The apparent crystallinities at the end of the respective experiments (w_c) for the three lower T_c's were near 70% (see Table 2), while that of PEO crystallized at 52 °C was near 60%. The values for the three lowest T_c's are almost the same within the experimental uncertainty to those determined from differential scanning calorimetry (DSC) experiments conducted on samples taken from the WAXD/SAXS specimens after

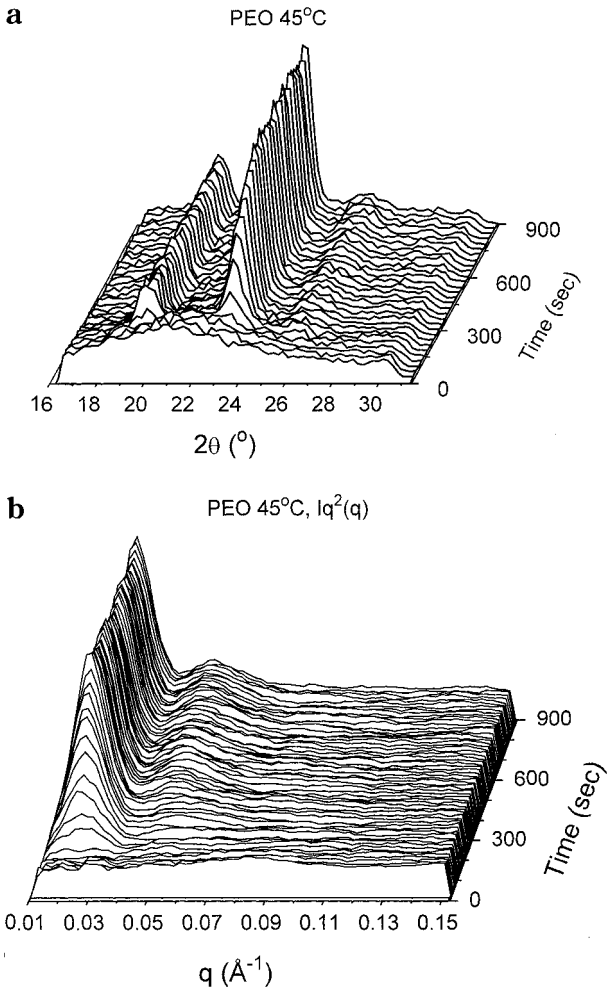

Figure 1. (a) Development of the WAXD and (b) Lorentz-corrected SAXS profiles as a function of crystallization time for PEO at $T_c = 45$ °C. 2θ is relative to $\lambda = 0.154$ nm.

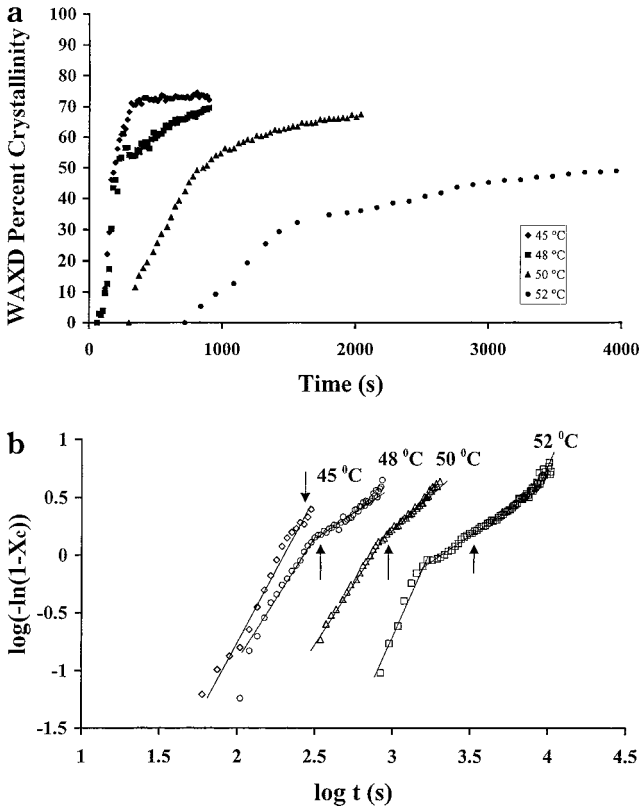

Figure 2. (a) Development of WAXD crystallinity as a function of crystallization time for neat PEO. The data for $T_c = 52$ °C continue out to ~10 500 s but are only shown through 4000 s to allow the data for the lower T_c's to be seen more clearly. (b) Avrami plots for PEO crystallized at various T_c's.

Table 2. Avrami Parameters for PEO from Time-Resolved WAXD

T_c (°C)	$t_{1/2}$ (s)	w_c (%)	z	n	X_{cs}[a]
45	180	75	2.6×10^{-6}	2.4	
48	220	70	3.4×10^{-7}	2.7	70
			3.5×10^{-3}	1.0	
50	610	67	5.9×10^{-7}	2.2	67
			1.2×10^{-4}	1.3	
52	1420	59	2.0×10^{-11}	3.3	60
			9.2×10^{-4}	0.9	

[a] X_{cs} = relative crystallinity at the end of the step.

cooling to room temperature and storage for several weeks. The DSC crystallinity of the specimen crystallized at 52 °C (~69%, based on a perfect crystal heat of fusion value of 203 J/g[15]) was somewhat higher than the final apparent WAXD value, likely indicating some additional crystallization on cooling to, and on storage at, room temperature.

It is evident from Figure 2 that there are at least two stages to the crystallization process at $T_c \geq 48$ °C for the PEO used in our experiments. This is clearly seen in Figure 2b, which is plotted in the classic double-log Avrami form. The phenomenological Avrami equation can be written as[16]

$$1 - X_c = \exp(-zt^n) \qquad (3)$$

where X_c is the fraction crystallized at time t ($X_c = 1$ at the conclusion of crystallization), z is a constant dependent on nucleation and growth rates, and n is related to the type of nucleation and growth geometry. Selected, fitted n and z values are provided throughout the text as a convenient way to compare the crystallization behavior of the various materials.

Given the modest number of data points available for PEO crystallized at 45 °C and considering the experimental uncertainty in the measured WAXD crystallinities, a single Avrami expression is fitted through the experimental data. A minimum of two Avrami expressions are required to adequately fit the data at $T_c \geq 48$ °C. This is not surprising in that it has been reported that a single Avrami process is insufficient for fitting the experimental crystallization data of many polymers (e.g., refs 17 and 18). As seen in Table 2, values of n for the dominate first process (encompassing the first 60−70% of the crystallization process) are between 2 and 3 (roughly consistent with the expectation of spherulitic crystallization), while those of the second process are near 1. These values are remarkably similar to those reported previously in a DSC study of a binary mixture of low and high PEO molecular weight fractions,[19] and it was argued that molecular segregation of the lower molecular weight species was responsible for the longer time process. A value of $n \sim 1$ for the second process has been associated with rodlike growth, nucleated on existing crystal surfaces.[20] Recall that the PEO used in our experiments is relatively polydisperse, and molecular weight fractionation is therefore a plausible origin for the second, longer time process seen in Figure 2. There also appears to be a third process at the longest crystallization times at $T_c = 52$ °C, occurring over the

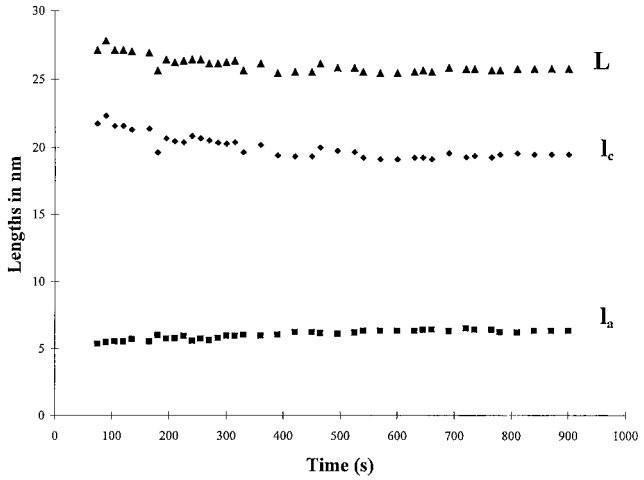

Figure 3. Crystallization time dependence of the average long period, lamellar thickness, and amorphous layer thickness in lamellar stacks for PEO crystallized at 48 °C.

Table 3. Microstructural Parameters at the Conclusion of Crystallization for Neat PEO from SAXS

T_c (°C)	L (nm)	l_c (nm)	l_a (nm)
45	25.2	19.3	5.9
48	25.7	19.5	6.2
50	31.0	23.8	7.2
52	32.7	25.5	7.2

last ~5% of the crystallization process. The origin of this is unknown at the present time.

The values for the microstructural parameters determined from the simultaneous SAXS experiments at the conclusion of the crystallization experiments are summarized in Table 3. As expected, l_c and the long period increase significantly with increasing T_c, and the values compare favorably to those determined previously in "static" SAXS experiments.[1]

Average long periods and lamellar thicknesses were found to decrease at early crystallization times at all T_c's and then remain constant throughout the duration of crystallization.[21] For example, the behavior of PEO crystallized at 48 °C is shown in Figure 3. The initial decrease in L and l_c was about 2−3 nm at each T_c. The crystallization time at which L and l_c become time independent is noted in Figure 2b by the arrows. This is very near the conclusion of crystallization at $T_c = 45$ °C and near the "break" in the data corresponding to the change from $n \sim 2-3$ to $n \sim 1$ (i.e., to the dominance of "secondary" crystallization) for $T_c = 48$ and 50 °C (and to a rough approximation, for 52 °C). Similar behavior has been observed during crystallization of other polymers.[23,24] The implication is that lamellar insertion processes (see below), for example, continue throughout primary crystallization.

A modest decrease in the mean L and l_c during the first portion of the crystallization process has been reported for a number of different polymers (e.g., refs 25 and 26), while lamellar *thickening* during isothermal crystallization has been reported for polyethylene.[27] There has been some speculation that the difference in behavior is associated with chain flexibility (i.e., more flexible chains are able to rearrange or "perfect" more easily), but this does not appear to be the case considering the behavior of flexible PEO. Putting this another way, the behavior does not appear to be associated with higher crystallization (reorganization) rates since high molecular weight PEO crystallizes more rapidly than

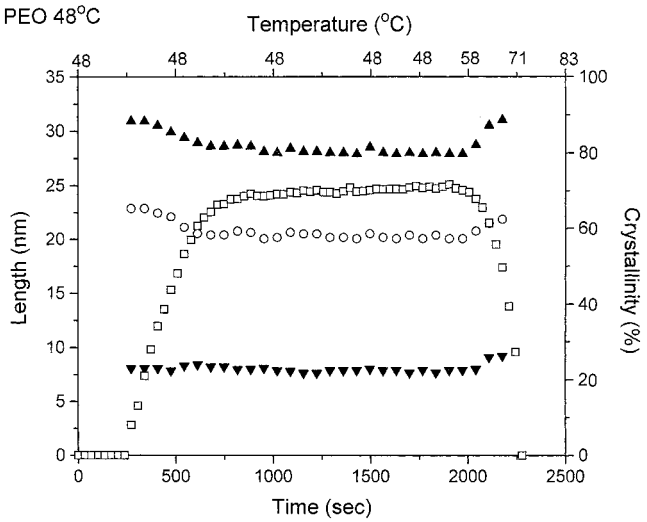

Figure 4. SAXS microstructural parameters and WAXD crystallinities as a function of time for PEO during crystallization at $T_c = 48$ °C and then as a function of temperature during melting at 3 °C/min after crystallization: □, WAXD crystallinity; ▲, long period; ○, lamellar thickness; ▼, amorphous layer thickness.

linear polyethylene, at equivalent degrees of supercooling and molecular weight.[28,29]

The origin of the initial decrease in L and l_c for PEO and other polymers remains uncertain. A frequent proposal is that this arises from insertion of subsidiary lamella within or between lamellar stacks during primary crystallization.[30,31] Others however have argued that it may arise from diminishing lamellar corrugation during crystallization[32] or from progressive thickening of lamellar stacks (although the latter argument apparently does not account for a reduction in mean l_c).[33]

To explore this issue further, we undertook a series of experiments on neat PEO crystallized at 45 and 48 °C. Crystallization was conducted for time periods well in excess of the time when the crystallinity became constant, and the samples were subsequently melted by ramping the temperature from T_c to 100 °C at 3 °C/min. The microstructural parameters from SAXS and the WAXD crystallinities for PEO crystallized at 48 °C are depicted in Figure 4. Neither the PEO crystallized at 45 or 48 °C is completely molten until the measured cell temperature is in excess of 71 °C, above the generally accepted T_m^0 for PEO (69 °C[34]). The apparent temperatures experienced by the PEO samples are artificially high as a consequence of thermal lag associated with the relatively large specimens used in the temperature jump experiments. This was confirmed in DSC experiments of samples taken directly from the WAXD/SAXS specimens. The DSC melting point (measured on small samples (~0.1 mg) to minimize thermal lag) was found to be near 62 °C, ~8−10 °C lower than the apparent value determined in the corresponding WAXD/SAXS experiment. Relatively large differences in the apparent T_m of specimens taken from the same sample of a low thermal conductivity crystalline polymer are not uncommon. For example, a sample from a melt-crystallized polyethylene taken in the form of a "large chunk" (~1.2 mg) was found to have a DSC melting point some 10 °C higher than a small, thin slice taken from the same specimen.[35]

As seen in Figure 4, as the temperature is ramped after crystallization is complete, the percent crystallinity

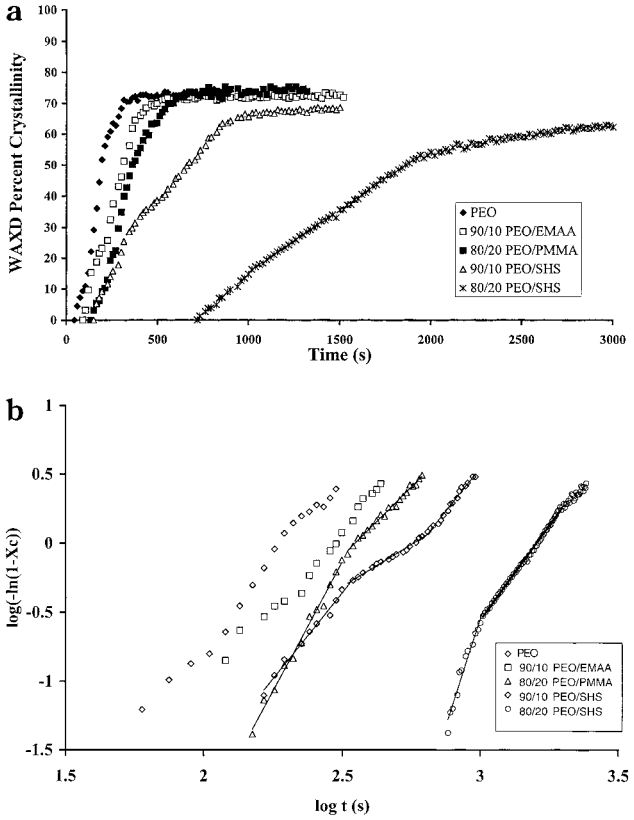

Figure 5. (a) WAXD crystallinity as a function of crystallization time for PEO and blends crystallized at 45 °C. (b) Avrami plots for PEO and blends crystallized at 45 °C.

gradually decreases and L, l_c, and l_a increase until the specimens are completely molten. Partial melting and recrystallization are often observed while heating crystalline polymers to their melting point (e.g., ref 36). If this were the case, one would expect L and l_c to increase at higher temperatures, consistent with the observations in Figure 4. However, we have conducted DSC melting experiments on these and other isothermally crystallized PEO samples; a single melting point is observed for samples crystallized at the T_c's of interest, and the melting endotherms exhibit little if any heating rate dependence. It therefore appears that a melting and recrystallization mechanism is not the origin of the behavior in Figure 4.

For a model involving insertion of thinner lamellar during crystallization, one would expect the thinner lamellae to melt first on subsequent heating. This would lead to an increase in mean L, l_c, and l_a (essentially the reverse of what is observed on crystallization), which is in general agreement with the observations in Figure 4.

PEO Blends. a. T_c = 45 °C. The time dependence of the WAXD crystallinity for PEO and selected blends crystallized at 45 °C is shown in Figure 5a, along with the corresponding Avrami plots in Figure 5b. As seen in the figures and from the crystallization half-times in Table 4 ($t_{1/2}$ is defined as the time when the relative crystallinity is 50%), the bulk crystallization rates generally conform to expectations from our earlier spherulite growth rate measurements.[3] For example, the blend containing 20% of the strongly interacting SHS copolymer crystallizes much more slowly than PEO or the corresponding blend with PMMA (by a factor of ~8 and 5, respectively). In addition to the usual diluent

Table 4. Avrami Parameters for PEO and Blends Crystallized at 45 °C from Time-Resolved WAXD

material	$t_{1/2}$ (s)	w_c (%)	z	n	X_{cs}[a]
PEO	180	75	2.6×10^{-6}	~2.4	
90/10 EMAA	250	72	3.6×10^{-6}	~2.2	
80/20 PMMA	300	75	3.0×10^{-10}	3.8	54
			9.3×10^{-6}	2.0	
90/10 SHS	400	68	3.4×10^{-7}	2.4	43
			6.8×10^{-4}	1.2	~72
			3.0×10^{-8}	2.7	
80/20 SHS	1360	62	9.4×10^{-21}	6.5	24
			4.4×10^{-9}	2.6	

[a] X_{cs} = relative crystallinity at the end of a step.

Table 5. Microstructural Parameters at the Conclusion of Crystallization at 45 °C from SAXS

material	L (nm)	l_c (nm)	l_a (nm)
PEO	25.2	19.3	5.9
80/20 PEO/PMMA	27.5	19.3[a]	8.2[a]
90/10 PEO/EMAA	26.9	20.6	6.3
90/10 PEO/SHS	27.2	19.5	7.7
80/20 PEO/SHS	32.1	24.5	7.6

[a] Calculated assuming $l_c = l_c$(PEO) at this T_c.

effect, this arises from a significant reduction in the equilibrium melting point for PEO in the strongly interacting mixtures, and hence crystallization proceeds at a significantly smaller ΔT for these blends. This is confirmed by examining the final lamellar thicknesses for the blends vs neat PEO (Table 5).

Previous work has shown that PMMA is trapped in regions between PEO lamellae during crystallization at the T_c's under consideration here (e.g., refs 1 and 37), leading to an increase in long period with increasing PMMA concentration. This results in a reduction of the linear stack crystallinity into the range where unique determination of l_c and l_a from $\gamma(r)$ is unreliable. However, since the interaction parameter is near zero for PMMA blends,[37] it is reasonable to expect the average lamellar thickness to be the same as that of PEO crystallized at the same T_c. This assumption was made in arriving at the l_a value for the PMMA blends in Table 5 (and 6).

For the 10% EMAA blend, there is a modest increase in l_c over that of neat PEO, while l_a remains the same within experimental uncertainty. This is in agreement with crystallization at a slightly lower ΔT than PEO and diffusion of EMAA into interfibrillar regions during the course of crystallization.[1] The SHS copolymer has a higher T_g, and its mobility is considerably more sluggish than EMAA. This is in line with the data in Table 5 that indicate that the increase in long period of the 10% SHS blend results primarily from interlamellar incorporation. At 20% SHS, a portion of the diluent polymer is incorporated within lamellar stacks, and a significant increase in lamellar thickness is observed due to a reduction in ΔT. In previous papers we estimated that the equilibrium melting point is depressed by ~6 °C for the 20% SHS blend.[1,3]

The time dependence of the SAXS microstructural parameters for the low T_g EMAA (as well as low T_g poly(vinyl acetate)) blends looks very much like that shown for neat PEO (seen in Figure 3). There is a decrease in long period and l_c of ~2−3 nm for both EMAA compositions at both T_c = 45 and 48 °C.

However, blends with higher T_g SHS and PMMA generally exhibit a more significant decrease in long period (~5−9 nm) during the early stages of crystal-

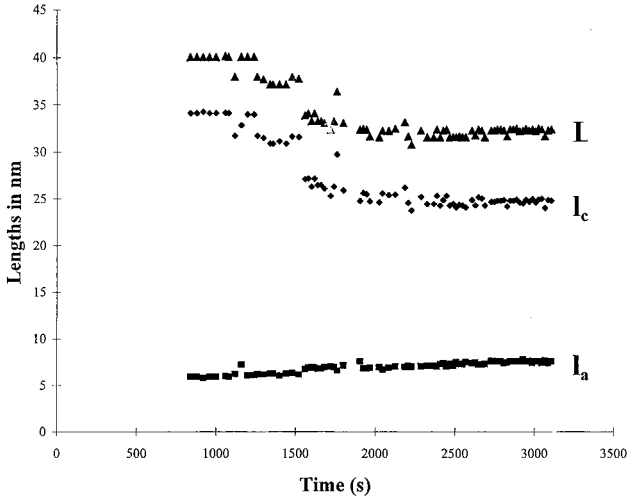

Figure 6. Dependence of the microstructural parameters on crystallization time for the 10% SHS blend crystallized at 45 °C.

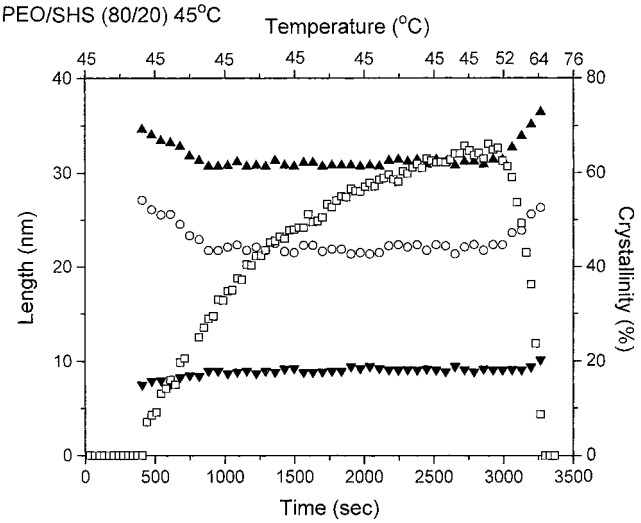

Figure 7. Microstructural parameters and WAXD crystallinities as a function of time during crystallization of the 20% SHS blend at $T_c = 45$ °C and then during melting at 3 °C/min after crystallization: □, WAXD crystallinity; ▲, long period; ○, lamellar thickness; ▼, amorphous layer thickness.

lization. This is accompanied by a corresponding large decrease in mean l_c with time for the SHS blends. A typical example is shown in Figure 6. Because of the difficulty in unambiguously determining l_c from the correlation function for the PMMA blends, we focus on the more comprehensive data for the SHS blends in attempting to formulate a model that accounts for these changes.

We have shown previously that higher T_g amorphous polymers can inhibit reorganization (lamellar thickening) of polymer crystals during heating.[38,39] A similar effect can be envisioned during crystallization. Crystallization may be relatively unrestricted at early crystallization times and the long period determined by thickened[21] lamellae ($l_c = \beta l_g^*$) and l_a. As crystallization proceeds, SHS (or PMMA) can raise the local T_g of the amorphous component surrounding the lamellae and inhibit the thickening process (at least to some extent), leading to a reduction in mean lamellar thickness and long period with crystallization time. Superimposed on this is the possibility of the crystallization of thinner lamellae in regions within or between stacks, as was concluded for crystallization of neat PEO.

To investigate this further, the 20% SHS blend was crystallized at $T_c = 45$ °C until the measured WAXD crystallinity became constant, and the sample was subsequently melted by heating from T_c to 100 °C at 3 °C/min. The microstructural parameters and WAXD crystallinities are depicted in Figure 7. As expected, although there is significant thermal lag, the apparent melting "point" for the strongly interacting SHS blend is significantly below that of neat PEO crystallized at the same T_c. As was the case for PEO, changes in long period, l_c, and l_a upon melting are more or less a mirror image of those that occur relatively early in the crystallization process. DSC experiments again provide no evidence for lamellar thickening during melting, and so it appears that the changes in microstructural parameters during melting (and, by inference, during crystallization) are dominated by melting (crystallization) of thinner lamellae within and/or between lamellar stacks.

WAXD degrees of crystallinity at the conclusion of the time-resolved experiments are shown in Table 4. After compensating for the weight of diluent in blend, the crystallinities are generally the same as that for neat PEO within experimental uncertainty (except for the 20% PMMA blend which exhibits relatively high apparent PEO crystallinity).

For the materials that crystallize most quickly at 45 °C [i.e., PEO and the 10% EMAA blend], only a modest number of data points could be acquired during the course of crystallization, and the crystallinity data were therefore fit with a single Avrami expression (see Table 4). The values for z and n in these two cases are relatively uncertain due to the scatter in the data points. Nevertheless, n falls between 2 and 3 for the 10% EMAA blend, as it does for neat PEO. For the somewhat more slowly crystallizing 20% PMMA mixture, two distinct processes are evident in Figure 5b: a relatively fast one through about 50% relative crystallinity (with n close to 4), followed by a slower process with $n \sim 2$. Two processes are also observed for the 20% SHS blend, although the change in kinetics occurs at a significantly lower value of the relative crystallinity (i.e., ~20% compared to ~50% for the PMMA blend). In addition, fitting the shorter time data results in a very large apparent n. The Avrami plot for the 10% SHS blend provides an indication of three distinct stages during the course of crystallization.

b. $T_c = 48$ °C. The time dependence of the WAXD crystallinities for the materials crystallized at 48 °C and the corresponding Avrami plots are shown in parts a and b of Figure 8, respectively. Again, the crystallization half-times are consistent with expectations from spherulite growth rate experiments, with the blends containing 15% EMAA and 20% SHS exhibiting particularly slow rates (i.e., ~7−10 times slower than neat PEO crystallized at 48 °C). The significant depression of the equilibrium melting point of PEO in these blends is consistent with the large increase in l_c (~10 nm, see Table 6).

The degrees of crystallinity (relative to PEO content) attained for the 10% EMAA and SHS blends are identical within experimental error to that of PEO. The values for the 15% EMAA and 20% SHS blends, however, are considerably smaller (59 and 52% crystallinity, based on the PEO concentration, vs 70% for neat PEO). This presumably results from restricted PEO crystallization in regions with high EMAA or SHS content.

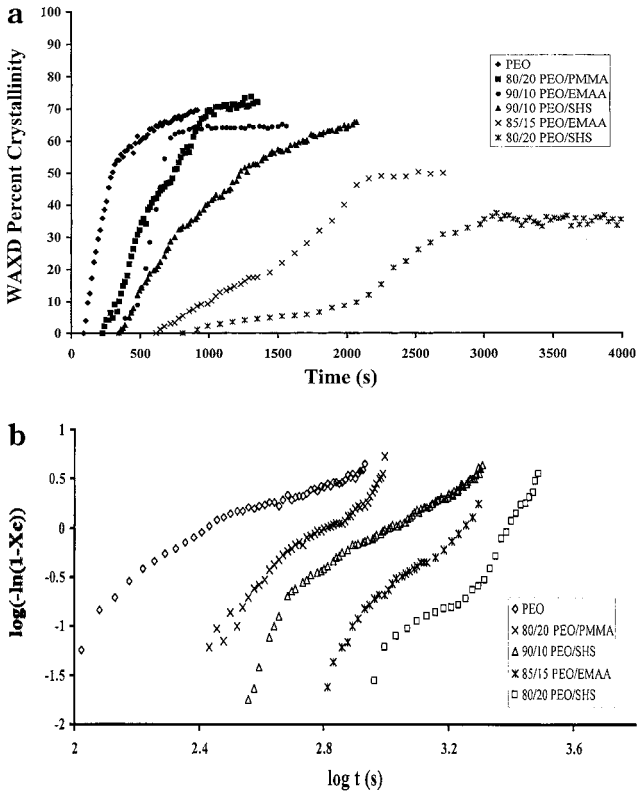

Figure 8. (a) WAXD crystallinity as a function of crystallization time for PEO and blends crystallized at 48 °C. (b) Avrami plots for PEO and blends crystallized at 48 °C.

Table 6. Microstructural Parameters at the Conclusion of Crystallization at 48 °C from SAXS

material	L (nm)	l_c (nm)	l_a (nm)
PEO	25.7	19.5	6.2
80/20 PEO/PMMA	29.7	19.5[a]	10.2[a]
90/10 PEO/EMAA	33.5	27.1	6.4
85/15 EMAA	34.9	28.3	6.6
90/10 PEO/SHS	29.8	22.3	7.5
80/20 PEO/SHS	37.1	30.2	6.9

[a] Calculated assuming $l_c = l_c$(PEO) at this T_c.

The average amorphous layer thickness in lamellar stacks for all EMMA blends (see Tables 5 and 6) is the same as PEO, supporting the view that EMAA diffuses over relatively long length scales during crystallization at these temperatures and resides primarily outside of lamellar stacks. The average l_a for SHS blends is somewhat larger than that of the appropriate PEO, indicating some entrapment of SHS chains within lamellar stacks, in line with the lower mobility of SHS vs EMAA. Since the crystallization time is considerably longer for the 20% SHS blend at 48 °C, there is more time for diffusion of SHS from the growth front and less overall SHS entrapment within stacks.

The time dependence of L, l_a, and l_c for the blends crystallized at 48 °C is the same as noted earlier: L and l_c decrease by about 2−3 nm at early crystallization times for the low T_g EMAA blends, while there is a more significant decrease (5−9 nm) for the higher T_g PMMA and SHS blends. Speculation regarding the origin of this behavior was presented in the previous subsection.

We finally come to the relatively complex crystallization behavior depicted in Figure 8a,b. To avoid overemphasizing specific fitted values for n and z, only general trends are discussed. There appear to be three crystallization processes for the blends crystallized at 48 °C. Like the case of the slowly crystallizing 20% SHS blend at 45 °C, the fitted n is very large (ca. 6−8) early in the crystallization process of blends containing strongly interacting polymers. There is then a transition to kinetics characterized by $n \sim 1-2$ in all cases, followed by a third process with higher n. The difficulty in assigning a specific origin to the kinetic data of the blends lies in the uncertainty of distinguishing the effects of PEO molecular weight segregation (which are anticipated on the basis of the results in the previous section) and contributions from fractionation and/or segregation of diluent molecules. A series of systematic experiments utilizing PEO and diluent polymers of well-defined (including narrow) molecular weight distributions are in progress in an attempt to shed some light on this complex behavior.

Conclusions

Our time-resolved, simultaneous WAXD/SAXS experiments have shown that the polydisperse PEO under consideration crystallizes in two distinct stages at the T_c's investigated. The first, dominant stage is characterized by an Avrami exponent in the range of 2−3, followed by a longer time process with $n \sim 1$. This behavior is very similar to that reported previously during crystallization of mixtures on PEO molecular weight fractions,[19] and it seems likely that molecular weight fractionation is responsible for the longer time process. A modest decrease in long period and lamellar thickness occurs during the first crystallization stage, similar to observations on other polymers (e.g., refs 23 and 24). The results of real-time WAXD/SAXS melting experiments, as well as separate DSC experiments, point to lamellar insertion within or between lamellar stacks as the likely origin of this behavior.

As expected, crystallization rates decreased significantly when melt-miscible diluent polymers were present, particularly when the diluent exhibits strong intermolecular interactions with PEO. The strong interactions lead to a significant reduction in equilibrium melting point and hence an increase in lamellar thickness when compared to neat PEO crystallized at the same T_c. The crystallization time dependence of the SAXS microstructural parameters for the blends is generally similar to that observed for PEO, with the exception that the magnitude of the initial decrease in L and l_c is significantly larger for blends containing higher T_g diluent polymers. Although inferences from real-time melting experiments indicate the importance of lamellar insertion, the role of the relatively high T_g diluents in inhibiting thickening of nascent lamellae is also expected to be significant.

The development of the bulk crystallinity of the blends is generally more complex than neat PEO. As many as three processes are observed, particularly for slowly crystallizing systems where diluent diffusion is expected to be an important consideration. Similar experiments are in progress on blends of narrow molecular weight fractions, which should allow removal/isolation of contributions from molecular weight segregation of the PEO and diluent polymer during crystallization.

Acknowledgment. The Penn State authors express their appreciation to the donors of the American Chemical Society−Petroleum Research Fund and the National Science Foundation (DMR-9900638) for their support of this research. B.H. and F.Y. thank a Department of

Energy grant (DEFG0299ER45760) for support of the AP−PRT beamline. We also thank Stephen Baratian and James Garrett for their assistance with the time-resolved experiments.

References and Notes

(1) Talibuddin, S.; Wu, L.; Runt, J.; Lin, J. S. *Macromolecules* **1996**, *29*, 7527.
(2) Talibuddin, S.; Runt, J.; Liu, L.-Z.; Chu, B. *Macromolecules* **1998**, *31*, 1627.
(3) Wu, L.; Lisowski, M. S.; Talibuddin, S.; Runt, J. *Macromolecules* **1999**, *32*, 1576.
(4) Keith, H. D.; Padden, F. J. *J. Appl. Phys.* **1964**, *35*, 1286.
(5) Keith, H. D.; Padden, F. J. *J. Polym. Sci., Polym. Phys. Ed.* **1987**, *25*, 2297.
(6) Cheung, Y. W.; Stein, R. S.; Chu, B.; Wu, G. *Macromolecules* **1994**, *27*, 3589.
(7) Liu, L.-Z.; Chu, B.; Penning, J. P.; St. John Manley, R. *Macromolecules* **1997**, *30*, 4398.
(8) Dreezen, G.; Mischenko, N.; Koch, M. H. J.; Reynaers, H.; Groeninckx, G. *Macromolecules* **1999**, *32*, 4015.
(9) Yeh, F.; Hsiao, B. S.; Chu, B.; Sauer, B. B.; Flexman, E. A. *J. Polym. Sci., Polym. Phys. Ed.* **1999**, *37*, 3115.
(10) Lee, J. Y.; Painter, P. C.; Coleman, M. M. *Macromolecules* **1988**, *21*, 346.
(11) Hsiao, B. S.; Chu, B.; Yeh, F. http://bnlx27c.nsls.bnl.gov (15 Apr 1997).
(12) Balta Calleja, F. J.; Vonk, C. G. *X-ray Scattering of Synthetic Polymers*; Elsevier: New York, 1989.
(13) Hsiao, B. S.; Verma, R. K. *J. Synchrontron Radiat.* **1998**, *5*, 23.
(14) Strobl, G. R.; Schneider, M. *J. Polym. Sci., Polym. Phys. Ed.* **1980**, *18*, 1343.
(15) Wunderlich, B. *Macromolecular Physics;* Academic Press: New York, 1980; Vol. 3.
(16) Avrami, M. *J. Chem. Phys.* **1939**, *7*, 1103.
(17) Wunderlich, B. *Macromolecular Physics;* Academic Press: New York, 1973; Vol. 1.
(18) Ravindranath, K.; Jog, J. P. *J. Appl. Polym. Sci.* **1993**, *49*, 1395.
(19) Cheng, S. Z. D.; Wunderlich, B. *J. Polym. Sci., Polym. Phys. Ed.* **1986**, *24*, 595.
(20) Akalu, Y.; Kielhorn, L.; Hsiao, B. S.; Stein, R. S.; Russell, T. P.; van Egmond, J.; Muthukumar, M. *Macromolecules* **1999**, *32*, 705.
(21) The generally accepted model of polymer crystallization (i.e., that of Hoffman, Lauritzen, and Miller[22]) envisions lamellar thickening by some factor (β) after formation of a crystal of initial thickness l_g*, resulting in a "final" $l_c = \beta l_g$*. Presumably, such thickening occurs very quickly, i.e., in the time frame that experimental data are acquired.
(22) Hoffman, J. D.; Miller, R. L. *Polymer* **1997**, *38*, 3151.
(23) Kruger, K. N.; Zachman, H. G. *Macromolecules* **1993**, *26*, 5202.
(24) Verma, R.; Marand, H.; Hsiao, B. *Macromolecules* **1996**, *29*, 7767.
(25) Hsiao, B. S.; Gardner, K. H.; Wu, D. Q.; Chu, B. *Polymer* **1993**, *34*, 3996.
(26) Jonas, A. M.; Russell, T. P.; Yoon, D. Y. *Macromolecules* **1995**, *28*, 8491.
(27) Albrecht, T.; Strobl, G. R. *Macromolecules* **1996**, *29*, 783.
(28) Cheng, S. Z. D.; Chen, J.; Janimak, J. J. *Polymer* **1990**, *31*, 1018.
(29) Hoffman, J. D.; Miller, R. L. *Polymer* **1997**, *38*, 3151.
(30) Lee, C. H.; Saito, H.; Inoue, T.; Nojima, S. *Macromolecules* **1996**, *29*, 7034.
(31) Bassett, D. C. *Philos. Trans. R. Soc. London A* **1994**, *348*, 29.
(32) Elsner, G.; Koch, M. H. J.; Borda, H. G.; Zachman, H. G. *Makromol. Chem.* **1981**, *182*, 1263.
(33) Ivanov, D. A.; Legras, R.; Jonas, A. M. *Macromolecules* **1999**, *32*, 1582.
(34) Cheng, S. Z. D.; Chen, J.; Janimak, J. J. *Polymer* **1990**, *31*, 1018.
(35) Harrison, I. R.; Varnell, W. D. *J. Therm. Anal.* **1982**, *25*, 391.
(36) Runt, J.; Harrison, I. R. In *Methods of Experimental Physics*; Fava, R., Ed.; Academic Press: New York, 1980; Vol. 16B, Chapter 9.
(37) Russell, T. P.; Ito, H.; Wignall, G. D. *Macromolecules* **1988**, *21*, 1703.
(38) Harrison, I. R.; Runt, J. *J. Polym. Sci., Polym. Phys. Ed.* **1980**, *18*, 2257.
(39) Runt, J. *Macromolecules* **1981**, *14*, 420.

MA000207C